Atmos. Chem. Phys., 14, 2789–2804, 2014
www.atmos-chem-phys.net/14/2789/2014/
doi:10.5194/acp-14-2789-2014

Atmospheric Chemistry and Physics Open Access

Suppression of new particle formation from monoterpene oxidation by NO_x

J. Wildt[1], T. F. Mentel[2], A. Kiendler-Scharr[2], T. Hoffmann[3], S. Andres[2], M. Ehn[2,*], E. Kleist[1], P. Müsgen[2,], F. Rohrer[2], Y. Rudich[4], M. Springer[2], R. Tillmann[2], and A. Wahner[2]**

[1]Institut für Bio- und Geowissenschaften, IBG-2, Forschungszentrum Jülich, 52425, Jülich, Germany
[2]Institut für Energie- und Klimaforschung, IEK-8, Forschungszentrum Jülich, 52425, Jülich, Germany
[3]Institut für Anorganische und Analytische Chemie, Johannes Gutenberg Universität Mainz, 55128, Mainz, Germany
[4]Weizmann Institute of Science, Rehovot, 76100, Israel
[*]now at: Department of Physics, Division of Atmospheric Sciences, Helsinki University, PL 64, 00014 Helsingin yliopisto, Finland
[**]now at: Frankenstrasse 8, 52382, Niederzier, Germany

Correspondence to: J. Wildt (j.wildt@fz-juelich.de)

Received: 25 June 2013 – Published in Atmos. Chem. Phys. Discuss.: 8 October 2013
Revised: 23 January 2014 – Accepted: 10 February 2014 – Published: 18 March 2014

Abstract. The impact of nitrogen oxides ($NO_x = NO + NO_2$) on new particle formation (NPF) and on photochemical ozone production from real plant volatile organic compound (BVOC) emissions was studied in a laboratory setup. At high NO_x conditions ($[BVOC]/[NO_x] < 7$, $[NO_x] > 23$ ppb) new particle formation was suppressed. Instead, photochemical ozone formation was observed resulting in higher hydroxyl radical (OH) and lower nitrogen monoxide (NO) concentrations. When [NO] was reduced back to levels below 1 ppb by OH reactions, NPF was observed. Adding high amounts of NO_x caused NPF to be slowed by orders of magnitude compared to analogous experiments at low NO_x conditions ($[NO_x] \sim 300$ ppt), although OH concentrations were higher. Varying NO_2 photolysis enabled showing that NO was responsible for suppression of NPF. This suggests that peroxy radicals are involved in NPF. The rates of NPF and photochemical ozone production were related by power law dependence with an exponent approaching −2. This exponent indicated that the overall peroxy radical concentration must have been similar when NPF occurred. Thus, permutation reactions of first-generation peroxy radicals cannot be the rate limiting step in NPF from monoterpene oxidation. It was concluded that permutation reactions of higher generation peroxy-radical-like intermediates limit the rate of new particle formation.

In contrast to the strong effects on the particle numbers, the formation of particle mass was substantially less sensitive to NO_x concentrations. If at all, yields were reduced by about an order of magnitude only at very high NO_x concentrations.

1 Introduction

Secondary organic aerosols (SOA) are an important component of tropospheric aerosols, affecting the radiation balance of Earth's atmosphere either directly by scattering or absorbing incoming sunlight or by acting as cloud condensation nuclei. Due to the strong biogenic sources of volatile organic compounds, a large fraction of SOA has natural sources. Plant emitted biogenic volatile organic compounds (BVOC) are oxidized in the atmosphere and the oxidation products condense on preexisting particulate matter, increasing their size and modifying their properties. New particle formation (NPF) has been frequently observed all over the world (Kulmala et al., 2004a), in clean background air (e.g., Dal Maso et al., 2007) as well as in urban atmospheres (e.g., Betha et al., 2013). Despite extensive studies, the mechanisms of NPF are not yet clarified. It is generally accepted that sulfuric acid (H_2SO_4) plays a key role in the formation of critical seed clusters (Kirkby et al., 2011). However, formation

of particulate matter with diameters above a few nanometers requires additional precursors (Kulmala et al., 2013).

Oxidized organic matter is postulated to be the complementary precursor to H_2SO_4 (Kulmala et al., 2004b; Metzger et al., 2010; Riipinen et al., 2011, 2012; R. Zhang et al., 2012; Kulmala et al., 2013). However, many oxidation steps are required for the formation of highly oxidized organic products with low enough vapor pressures that enable condensation onto critical clusters (Kiendler-Scharr et al., 2009; Ehn et al., 2010, 2012). The complexity of these oxidation steps hampers elucidating the basic processes of NPF.

Peroxy radicals (RO_2 with *R* representing the organic part + HO_2) are key intermediates in atmospheric chemistry because they are inevitable in reaction chains induced by the hydroxyl radical, OH. Peroxy radicals react with each other in multiple pairwise permutation reactions. The rates of those permutation reactions are controlled in a complicated manner and depend on the individual pair of peroxy radicals. As two peroxy radicals are involved in such reactions, the reaction rates depend on the concentrations of both peroxy radicals involved in the respective reaction.

Another important channel of peroxy radical reactions is the reaction with nitrogen monoxide, NO. RO_2 react with NO to form alkoxy radicals and NO_2. This reaction is the basis of photochemical ozone formation. The NO_2 molecule formed in the RO_2+ NO reaction is photolyzed by sunlight and the oxygen atom produced in this photolytic process directly forms ozone in a reaction with an oxygen molecule.

As a consequence of photochemical ozone formation peroxy radicals are consumed. Assuming that RO_2 consumption during photochemical ozone formation causes decreasing peroxy radical concentrations, photochemical ozone production will suppress the rates of permutation reactions of peroxy radicals among each other. In the presence of NO, products of permutation reactions are formed at lower rates than without NO in the system.

Effects of NO_x ($NO_x = NO + NO_2$) on particle formation were observed in several studies (e.g., Pandis et al., 1991; Presto et al., 2005b; Kroll et al., 2006; Zhang et al., 2006; Ng et al., 2007b; Kim et al., 2012) and the observed influence was generally attributed to impacts of RO_2+ NO reactions. However, quantitative data on the role of peroxy radicals in particle formation are scarce because measurements of peroxy radicals are difficult. Considering the basics of photochemical ozone formation, ozone production rates may be used as a tool to gain more insight into the role of peroxy radicals in particle formation: one peroxy radical is consumed per NO_2 formed in the $NO + RO_2$ reaction and, furthermore, one O_3 molecule is formed from the photolysis of one NO_2 molecule. Hence the rate of photochemical ozone production, $P(O_3)$, is a quantity that is linearly related to the consumption of peroxy radicals in reactions with NO. Consequently $P(O_3)$ can be used as a quantity giving hints to the suppression of permutation reaction rates.

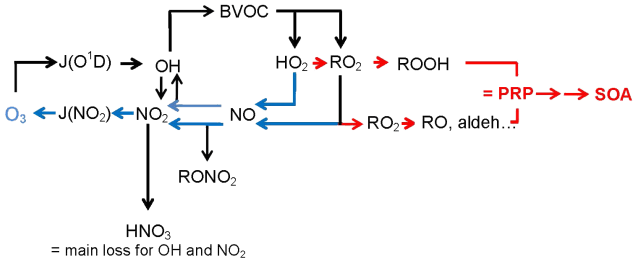

Fig. 1. Schematics of the basic reactions leading to SOA formation, considered in this study. BVOC oxidation forms peroxy radicals that, depending on the NO concentrations, have different fates. At low NO_x conditions, permutation reactions among RO_2 (including HO_2) are predominant (red arrows). Products of permutation reactions are termed PRP. At high NO_x conditions, peroxy radicals react predominantly with NO. Products of RO_2+ NO reactions are NO_2 and organic nitrates. NO_2 is photolyzed and subsequently O_3 is formed. On photolysis in the ultraviolet, O_3 is precursor of OH. Main sink of OH, the oxidant driving this chemistry, is the OH + NO_2 reaction. This reaction is also the main sink of NO_2 in the system.

To gain more insights into the role of peroxy radicals in NPF, we used $P(O_3)$ as a tool. We found that the photochemical system behaved more complicated than expectable from a simplistic approach: assuming that NPF would be controlled by permutation reactions of first-generation peroxy radicals led to contradictions. Our experimental results were unintelligible without considering higher generation oxidation products. However, basic peroxy radical photochemistry proved to be suitable for gaining hints about the character of rate limiting steps in NPF from monoterpene oxidation and to the chemical characteristics of nanoparticle precursors. A list of the acronyms used for better readability is given in the Appendix, Table A1.

2 Experimental

2.1 The Jülich Plant Atmosphere Chamber and instrumentation

Experiments were carried out in the Jülich Plant Atmosphere Chamber (JPAC). The setup is already described in detail (e.g., Mentel et al., 2009, 2013; Ehn et al., 2012). It consisted of two borosilicate glass chambers (volumes of 1150 and 1450 L) with Teflon floors mounted in separate climate chambers. Both chambers were operated as continuously stirred tank reactors (CSTR) with Teflon fans ensuring homogeneous mixing with mixing times of about 2 min. The smaller chamber contained the plants. A fraction of the air exiting this plant chamber was fed into the larger chamber that served as reaction chamber. Residence time of the air in the plant chamber was about 22 min; residence time of the air in the reaction chamber was about 63 min.

Air was purified by an adsorption dryer (KEA 70; Zander Aufbereitungstechnik GmbH & Co. KG, Essen, Germany) and by a palladium catalyst operating at 450 °C. Ozone, NO, NO_2, and volatile organic compounds (> C_3) were removed by the purification system. Concentrations of CO_2 and water vapor were further reduced by the adsorption dryer. By adding CO_2 from cylinders the CO_2 concentration in the chamber was kept at 350 ppm. The dew point in the plant chamber was restricted to a maximum of 13 °C to avoid condensation in the transfer line to the reaction chamber, which was at a temperature of 17 ± 0.5 °C.

Discharge lamps (HQI 400 W/D; Osram, Munich, Germany) were used to simulate the solar light spectrum in the plant chamber. At full illumination and at typical mid-canopy height photosynthetic photon flux density (PPFD) was 480 µmol m^{-2} s^{-1}. Infrared radiation (between 750 and 1050 nm) was reflected by filters (type IR3; Prinz Optics GmbH, Stromberg, Germany) placed between the lamps and the plant chamber in order to minimize radiative heating of the plants.

A fraction of the air leaving the plant chamber (~ 12 L min^{-1}) was fed into the reaction chamber. In addition, another air stream was introduced to the reaction chamber (~ 11 L min^{-1}). This second air stream was used to add O_3 to the reaction chamber and to maintain constant humidity in the chamber. O_3 was produced by O_2 photolysis at $\lambda = 189$ nm. By regulating the water vapor in the second air stream, the PPFD-dependent transpiration of the plants was compensated and the humidity in the reaction chamber was kept at 63 ± 1 %. The ozone inlet was placed opposite to the air inlet from the plant chamber to prevent immediate nucleation at uncontrolled conditions.

The reaction chamber was equipped with the same HQI 400 W/D lamps as the plant chamber. The HQI lamps had a spectrum similar to sunlight but with low intensity in the near UV (ultraviolet). To obtain sufficient NO_2 photolysis frequencies ($J(NO_2)$) another 12 discharge lamps (Phillips, TL 60 W/10-R, 60W, $\lambda_{max} = 365$ nm, from here on termed UVA lamps) were used. During the measurements described here, the reaction chamber was illuminated with 2 of the HQI 400 W/D lamps and all 12 UVA Lamps resulting in an NO_2 photolysis frequency of $J(NO_2) = 4.3 \times 10^{-3}$ s^{-1}. These lamps were installed outside of the reaction chamber. Due to the thick glass walls, light with wavelengths shorter than 350 nm was absent in the chamber.

OH radicals were generated by O_3 photolysis and reaction of the O^1D-atoms with water vapor. As efficient ozone photolysis in the Hartley band requires wavelengths shorter than 350 nm, a UVC lamp was installed inside the reaction chamber (Philips, TUV 40 W, $\lambda_{max} = 254$ nm, from here on termed as TUV lamp). Whenever the TUV lamp was switched on, OH radicals were generated at concentrations $> 10^7$ cm^{-3}. These concentrations are much higher than the OH concentrations expected as a byproduct of BVOC ozonolysis with the TUV lamp switched off. In the following we will always refer to the photolytical generated OH radicals, although there were always some OH radicals in the reaction system. The TUV lamp was shielded by glass tubes imposed on the lamp with a gap between the glass tubes. The photolytical OH production was adjusted by varying this gap. During the experiments described here $J(O^1D)$ was constant at about 9×10^{-4} s^{-1}. NO_2 photolysis by the TUV lamp was negligible but HNO_3 was photolyzed leading to a background of ~ 300 ppt NO_x (see below).

Nitrogen monoxide (Linde, 99.5 ± 5 ppm NO in nitrogen) was added to the air introduced from the plant chamber into the reaction chamber. The NO_x concentrations in the reaction chamber were varied between 0.3 and 103.5 ppb. Adding high amounts of NO caused a subsequent decrease of ozone concentrations in the chamber. Therefore, the ozone input was adjusted to obtain similar ozone concentrations when starting experiments. Without ozone photolysis, its concentration in the reaction chamber varied between 49 and 68 ppb when experiments started.

The UVA lamps were switched on long before the TUV lamp was switched on. Without the TUV light i.e., in the absence of high OH concentrations [NO], [NO_2] and [O_3] were near the photostationary steady state (PSS). At high NO_x conditions, ozone concentrations increased after switching on the TUV lamp. As NO_2 photolysis by the TUV lamp was inefficient, the increases of [O_3] in the chamber were due to photochemical ozone production and not due to variation of $J(NO_2)$. Based on differences of ozone concentrations between the chamber inlet and outlet, respectively, the rates of photochemical ozone production ($P(O_3)$) were determined (for more details see Supplement Sect. S2).

Trace gases were measured using commercial equipment. Ozone concentrations were determined by UV absorption (Thermo Environmental instruments, model 49), NO was measured by chemiluminescence (Eco Physics, CLD 770 AL ppt), and NO_2 by chemiluminescence after photolysis (Eco Physics, PLC 760). Two different systems were used. During a first period of the measurements a system with a detection limit of ~ 200 ppt at integration times of 100 s was used. During the later phases we were able to provide a system with an improved detection limit of ~ 10 ppt at 30 s integration time. Mixing ratios of BVOCs in plant chamber and reaction chamber were determined by measurements at the outlets of the respective chambers. These measurements were conducted using gas chromatography–mass spectrometry (GC-MS) and a proton transfer reaction mass spectrometer (PTR-MS, Ionicon, Innsbruck, Austria). The PTR-MS was switched continuously between the outlet of the plant chamber and the outlet of the reaction chamber to cross check the GC-MS data at higher time resolution. The GC-MS systems (Agilent GC-MSD-system HP5890 Series II + HP5972A MSD, GC-MSD-system HP6890 + 5973 MSD) had a similar configuration and were equipped with thermo-desorption systems (online

TDSG, Gerstel, Mülheim, Germany). For more details on the systems see e.g., Heiden et al. (2003).

The GC-MS system operated at plant chamber outlet was used to quantify the BVOCs introduced into reaction chamber. Note that the concentration of BVOCs introduced into the reaction chamber was smaller than measured at the outlet of the plant chamber because of the second air flow into reaction chamber. For all BVOC values given here this dilution was always considered.

The GC-MS operated at the outlet of the reaction chamber was used to quantify OH concentrations by measuring the decrease of certain BVOCs. During the experiments with plants we used α-pinene and β-pinene to determine OH concentrations. With the onset of O_3 photolysis the concentrations of both BVOCs decreased substantially but were still measurable. Using the rate constants of their reactions with OH (α-pinene $= 5.37 \times 10^{-11}$ cm^3 s^{-1}, β-pinene $= 7.89 \times 10^{-11}$ cm^3 s^{-1}, Atkinson, 1997) the OH concentrations were determined. The difference between the results obtained for [OH] using either of them was used as the uncertainty in [OH] (~ 20 %). For further details on OH measurements see Supplement to Kiendler-Scharr et al. (2009).

A condensation particle counter (CPC, 3022A, TSI) was directly connected to the reaction chamber by a straight stainless steel tube (diameter: 6 mm, length: 0.5 m). This CPC had a nominal activation diameter of 7 nm and was used to count the total number of particles formed in the chamber. A scanning mobility particle sizer (SMPS, TSI3081+TSI3786) also directly coupled to the reaction chamber measured the number–size distribution between 10 and 500 nm. The obtained size distributions were converted into volume distributions to determine particle volume and mass yields.

The yield of particle formation was related to the total BVOC consumption, given by the difference between inlet and outlet of the reaction chamber. Thus, the yield considers also the consumption of BVOCs by ozone reactions for particle mass formation. Nucleation rates (J_7) were determined from the first derivative of particle number concentrations as a function of time. The particle counter was sensitive only to particles that had already reached diameters of about 7 nm. Assuming these small particles to be spherical and having a density of ~ 1.2 g cm^{-3}, the masses of such 7 nm particles are in the range of ~ 1000 monoterpene masses. In the context used here, J_7 does not mean the formation rate of critical clusters but shows the appearance of small particles that already comprise of many molecules that have participated in early particle formation.

Direct plant emissions were used as SOA precursor because these are realistic BVOC mixtures making the results of such experiments independent of specific effects of individual BVOCs. Plants were delivered from Israel (details see Lang-Yona et al., 2010) and stored in a growth room before the measurements. The plant chamber contained five 3–4 year old tree seedlings: two Aleppo pines (*Pinus halepensis* L.), one holm oak (*Quercus ilex* L.), one Palestine oak (*Quercus calliprinos* L.), and one pistachio (*Pistacia palaestina* L.). A diurnal light cycle was simulated in the plant chamber by switching on and off the HQI lamps (06:00–18:00 LT (all times given in local time) full illumination, 18:00–19:00 simulation of twilight by switching off individual lamps, 19:00–05:00 darkness, and 05:00–06:00 simulation of twilight by switching on individual lamps). Not later than 3 h after twilight in the morning the VOC emissions from the plants were quite constant and another 3 h later conditions in the reaction chamber were near steady state. Then the TUV lamp was switched on to induce OH production and particle formation. One measurement was conducted per day with NO_x addition every second day.

In some experiments α-pinene was used as sole SOA precursor by using air from a permeation/diffusion source instead of the air from the plant chamber. Details of this source are described in Mentel et al. (2009). Furthermore, [OH] was determined using the decay of α-pinene alone. Otherwise the experimental procedure was the same as during the experiments with plant emitted BVOC.

2.2 Performance of the setup with respect to NO_x and nomenclature of BVOC / NO_x ratios

The reaction chamber was equipped with a 4 cm thick Teflon plate at the bottom. In particular for HNO_3 this Teflon plate acted as buffer. When NO_x was added to the reaction chamber, HNO_3 produced in reactions of NO_2 with OH diffused into the plate. The next day, when NO_x was removed from the air at the chamber inlet, HNO_3 diffused out of the plate. As HNO_3 was photolyzed at 254 nm, NO_x was produced in the reaction chamber. Together with some NO emitted from the plants, the NO_x production by HNO_3 photolysis determined a lower limit of around 300 ppt NO_x in the chamber. Hence we performed measurements at low NO_x conditions but no measurements at zero NO_x.

When OH was produced and BVOC concentrations decreased, NO_x concentrations also decreased due to reactions with OH. In accordance with Pandis et al. (1991) and related publications we will parameterize our experiments by $[NO_x]_0$, the initial NO_x concentrations in the reaction chamber before OH production. In case of the experiments without NO_x addition, $[NO_x]_0$ was set to 300 ppt, i.e., the NO_x concentration measured shortly after the TUV lamp was switched on and HNO_3 was photolyzed. For comparison with literature data we use the parameter $[BVOC]_0 / [NO_x]_0$ in units of [ppb C ppb^{-1}], abbreviated as BNR.

3 Methods: peroxy radicals and their reaction system

Details of the photochemical system, the chemical reactions and the derivation of the equations are given in the Supplement (Sect. S1). For better comparability, numbering of reactions and rate constants is adapted to that in the Supplement.

Peroxy radicals (RO_2+ HO_2) are key species in the photochemical system of interest. Figure 1 illustrates the known reactions of peroxy radicals as well as their trend with changing NO_x concentrations in the reaction system. Added is a pathway from permutation reactions to particle formation. Such pathway was suggested before for the growth of particulate matter (e.g., Kroll et al., 2006). Note that the notation RO_2 represents all individual ${RO_2}^i$ and $[RO_2]$ serves as abbreviation for the sum $\sum_i([{RO_2}^i])$. The same holds for the notations $RONO_2$, RO, ROOH, etc.

Reaction (R2) (Reaction R2 = Reaction R2a + Reaction R2b with rate constants k_{2a} and k_{2b}) is the major loss pathway for RO_2 at high NO_x conditions:

$$NO + RO_2 \xrightarrow{k_{2a}} RO + NO_2, \quad \text{(R2a)}$$

$$NO + RO_2 \xrightarrow{k_{2b}} RONO_2, \quad \text{(R2b)}$$

and leads to the formation of RO and NO_2 in Reaction (R2a) and to the formation of organic nitrates ($RONO_2$) in Reaction (R2b). Upon NO_2 photolysis ozone is formed.

The sum of the rate constants k_{2a} and k_{2b} (k_2), is the average rate constant for the reaction of NO with RO_2. The branching ratios for ozone formation and organic nitrate formation in Reaction (R2) are termed $Y(O_3)$ and $Y(RONO_2)$, respectively.

Reaction (R3) (R3 = R3a + R3b) is the main loss for RO_2 radicals at low NO_x conditions:

$$RO_2 + HO_2 \xrightarrow{k_{3a}} ROOH, \quad \text{(R3a)}$$

$$RO_2 + R'O_2 \xrightarrow{k_{3b}} RO, ROH, ROOR', \ldots. \quad \text{(R3b)}$$

Reaction (R3a) forms hydroperoxides. Reaction (R3b) forms different products including alkoxy radicals, alcohols, carbonyl compounds, etc. (e.g., master chemical mechanism, MCM for α-pinene), and probably also alkyl peroxides ROOR′ (e.g., Hallquist et al., 2009). The formation of ROOH can be considered as a special case of ROOR′ formation with R′ = H. In reaction R3 different peroxy radicals (RO_2 and HO_2) react with each other with permutation of all pairs being possible a priori. Reaction (R3) is therefore termed "permutation reaction". An average rate constant k_3 can be specified for a given reaction system of RO_2 and HO_2. Products of Reaction (R3) will be termed as permutation reaction products, PRP, and their production rates as P(PRP). If PRP are involved in NPF, NO will switch a photochemical system containing BVOC into either O_3 formation or new particle formation.

The photochemical system switches between P(PRP) and $P(O_3)$. Considering that the chemical systems were quite similar this switch was approximated by Eq. (1) (for details see Supplement, Eq. (1) is identical to Eq. (ES11) in the Supplement):

$$-\frac{\partial\left(\frac{P(PRP)}{P(O_3)}\right)}{\partial[NO]} = \text{const} \cdot \frac{[RO_2]}{[NO]^2}. \quad (1)$$

In Eq. (1), const is a constant. Varying [NO] leads to complex relationships between $P(O_3)$ and P(PRP), and eventually to particle formation. If $[RO_2]$ is constant, P(PRP) and $P(O_3)$ are related by an inverse power law dependence with an exponent close to −2 (for details see Supplement, Sect. 1). During our experiments we found power law dependence in this range.

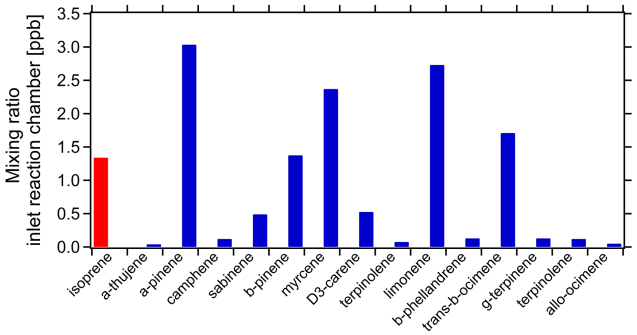

Fig. 2. BVOC mixing ratios at the inlet of the reaction chamber. Dilution by the second air stream is already considered, the sum of mixing ratios represents $[BVOC]_0$. The plants in the plant chamber (two Aleppo pines, one holm oak, one Palestine oak, and one pistachio) constitutively emitted isoprene (red bar) and monoterpenes (blue bars).

4 Results

4.1 BVOC emissions

The main emissions from the Mediterranean plants were those of monoterpenes (MT). Isoprene emissions were substantially lower and emissions of other biogenic VOCs were negligible. Figure 2 shows the emission pattern expressed as mixing ratios of BVOC introduced into the reaction chamber. During the 26 experiments conducted within about a month, day to day fluctuations in the plants' emissions were unavoidable. The BVOC concentrations introduced into the reaction chamber varied between ∼ 77 ppb C and ∼ 130 ppb C (∼ 44 to ∼ 73 µg m^{-3}). Although contributions of isoprene were always less than 10 % they were always considered in summing up BVOC concentrations. The sum of mixing ratios of the individual BVOC fed into the reaction chamber ($[BVOC]_0$) is listed in the second column of Table 1.

Due to the BVOC + O_3 reaction, the actual BVOC concentrations in the reaction chamber were lower than $[BVOC]_0$. In absence of photolytic OH production, BVOC concentrations decreased by a few percent for, e.g., camphene or

Table 1. Results from experiments with respect to particle formation from OH initiated oxidation of BVOC emitted from Mediterranean tree species.

BNR [ppb C] [ppb]$^{-1}$	$[BVOC]_0$ [ppb C]	$[NO_x]_0$ [ppb]	$[OH]/10^7$ [cm^{-3}][a]	J_7 [cm^{-3} s^{-1}]	PM_{max} [µg m^{-3}]	J_7/PM_{max} [cm^{-3} s^{-1} µg^{-1} m^3]	$P(O_3)$ [ppb h^{-1}]
1.1	119	103.5	0.28	0.13	0.08	1.5	62.9
1.8	122	69	0.47	0.23	0.28	0.82	66.8
3.2	124.5	39.4	0.54	0.17	3.80	0.46	31.9
4.3	98.5	23.1	[b]	3.4	[b]	[b]	24.1
8.9	109.5	12.3	1.68	9.2	3.97	2.32	4.3
10.2	104.3	10.2	1.89	14.3	4.18	3.41	0.1
12.8	105	8.2	[b]	23.6	4.50	5.3	−0.25
14.4	106.3	7.4	1.91	22.8	3.63	6.29	−1.39
18.0	88.3	4.9	1.83	22.1	2.00	11.0	−1.34
24.4	79.8	3.3	1.71	38.3	2.06	16.4	−5.77
25.4	124.5	4.9	1.47	63.9	5.00	12.77	1.56
28.6	117	4.1	1.71	57.4	4.00	14.4	−0.52
29.8	97.5	3.3	1.68	56.9	4.05	14.1	−3.13
61.1	100	1.64	1.40	45.7	4.71	9.71	−0.65
62.0	101.5	1.63	[b]	85.1	3.69	23.1	−2.58
79.2	129.5	1.6	0.99	104.3	7.00	14.9	2.00
255.8	76.8	0.3	[b]	64.1	1.57	40.9	1.81
277.5	83.3	0.3	1.58	43.0	1.53	28.1	1.11
300.0	90	0.3	1.59	61.4	3.52	17.4	2.17
326.7	98	0.3	1.06	43.4	3.10	14.0	−3.99
329.2	98.8	0.3	[b]	100.3	3.23	31.1	1.72
345.8	103.8	0.3	1.16	91.7	3.97	23.1	−1.05
363.8	109	0.3	[b]	84.2	3.67	22.9	−4.38
412.5	124	0.3	[b]	39.7	4.56	8.7	−0.43
414.2	124.3	0.3	1.11	62.3	5.70	10.9	−1.20
415.0	124.5	0.3	[b]	69.1	4.00	17.3	2.72

[a]Data for the first hour after switching on the TUV lamp, numbers in columns have to be multiplied by 10^7 to obtain OH concentrations in units of cubic centimeters. [b]No data due to failure of respective equipment.

β-pinene and up to more than 90% for, e.g., myrcene. When OH was generated, BVOC concentrations decreased further. For example, during low NO_x experiments, the α-pinene concentrations in the reaction chamber were at maximum 200 ppt indicating that more than 95 % of the α-pinene was oxidized. At high NO_x conditions ($[NO_x] > 30$ ppb) α-pinene concentrations at the chamber outlet were in the range of several hundreds of parts per trillion for the first hours. In the course of such experiments the α-pinene- and β-pinene concentrations decreased to ~ 20 ppt because OH concentrations increased with time. Nevertheless, in nearly all measurements, α-pinene and β-pinene concentrations remained high enough to allow reasonable determinations of OH concentrations.

Because the isoprene contribution was less than 10 % and fairly constant from experiment to experiment, the suppressing impact of isoprene on new particle formation (see Kiendler-Scharr et al., 2009) was low. In the following analyses the impact of isoprene was neglected for the interpretation of NO_x impacts on NPF.

4.2 NO_x dependence of ozone- and new-particle formation

Figure 3 shows the temporal development of particle number density for three experiments with different $[NO_x]_0$. Two

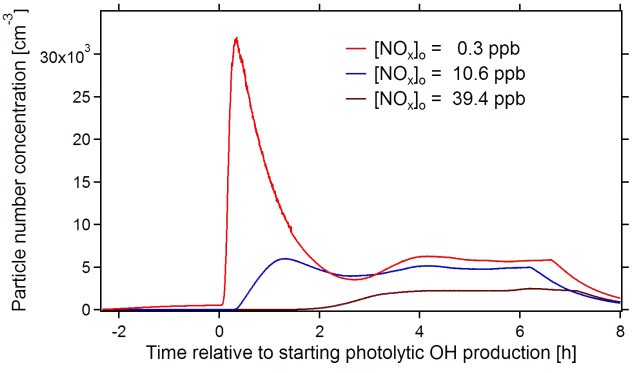

Fig. 3. Temporal shape of particle number concentrations for different $[NO_x]_0$. The sharp decrease of particle number concentration observed 6–8 h after inducing particle formation by OH production was caused by switching off the OH production and subsequent particle formation.

striking observations were made. The first was a decrease of maximum particle number concentration with increasing NO_x indicating a decrease of J_7. The second was a delay between the start of photolytic OH production and the onset of NPF. During long lag times $[NO_x]$, $[O_3]$ and [OH] systematically changed with time. While $[NO_x]$ decreased, $[O_3]$ and [OH] increased (see Fig. 4).

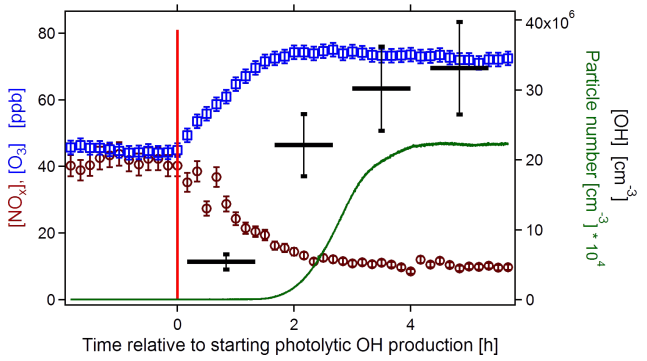

Fig. 4. Temporal behavior of [NO_x] (brown circles, left scale, ±8 %), [O_3] (blue squares, left scale, ±2 ppb), particle number concentration (green line, right scale, multiplied by 10^4 for clarity), and [OH] (black bars, right scale, ±20 %) in an experiment with $[NO_x]_0 \sim 40$ ppb, $[BVOC]_0 \sim 124.5$ ppb C. OH concentrations were measured indirectly by GC-MS with a time resolution of ∼ 70 min. The red bar shows the time when the TUV lamp was switched on.

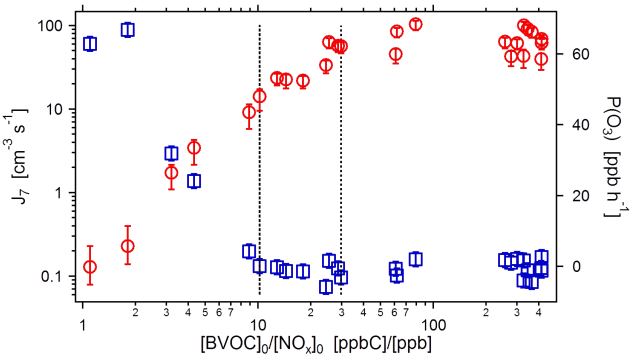

Fig. 5. Rates of new particle formation (J_7, red circles, left scale) and rates of photochemical ozone formation ($P(O_3)$, blue squares, right scale) in dependence of BNR. The cluster at high BNR stems from measurements without NO_x addition. The dashed lines show the region 30 > BNR > 10 where J_7 decreased by an order of magnitude but $P(O_3)$ stayed low. Note the logarithmic scale for J_7 and the linear scale for $P(O_3)$. Errors in $P(O_3)$ were estimated to be ±2.5 ppb h^{-1}. Errors in J_7 due to wall losses and background particle numbers were estimated as described in Sect. S7 of the Supplement.

For 1.1 < BNR < 10, rates of NPF and $P(O_3)$ were inversely related. With increasing BNR, J_7 increased by two orders of magnitude whereas $P(O_3)$ decreased from ∼ 60 ppb h^{-1} to nonmeasurable values (Fig. 5). In low NO_x regimes with 10 < BNR < 30 $P(O_3)$ was negligible while J_7 increased further by one order of magnitude. For BNR > 30 both, J_7 and $P(O_3)$ were insensitive to BNR.

Assuming power law dependencies for $J_7 = f(BNR)$ in the range 1.1 < BNR < 30 and for $P(O_3) = f(BNR)$ in the range 1.1 < BNR < 10 we derived an exponent of 1.9 ± 0.1, $R^2 = 0.97$, for J_7 and of −1.28 ± 0.3, $R^2 = 0.87$, for $P(O_3)$, respectively (further details in Supplement Sect. S3).

New particle formation is strongly dependent on OH concentration (Kiendler-Scharr et al., 2009). Figure 6 shows the OH concentrations as a function of $[NO_x]_0$ measured during the first hour after switching on the TUV lamp. The data for [OH] showed some scatter due to varying $[BVOC]_0$ but no significant decrease with increasing $[NO_x]_0$ up to about 20 ppb (BNR = 4.3). Only at $[NO_x]_0 > 30$ ppb [OH] dropped significantly below the range of values measured for $[NO_x]_0 < 30$ ppb. In the experiments with $[NO_x]_0 > 30$ ppb we observed also significant $P(O_3)$ as well as long lag times between the OH production and NPF.

In high $[NO_x]_0$ experiments, the OH production rates increased with time due to increases of [O_3]. Subsequent increases of [OH] caused decreases of [NO_x] (compare with Fig. 4). At the onset of NPF in high $[NO_x]_0$ experiments, [OH] was much higher than during the first hour of the experiment and [NO_x] was much lower than $[NO_x]_0$. This is demonstrated by the red square in Fig. 6 for $[NO_x]_0 = 103.5$ ppb, where [NO_x] dropped to 25 ppb and OH increased from 2.6×10^6 to 25×10^6 cm^{-3}.

4.3 Impact of NO_x on the SOA mass yield

To probe the impact of NO_x on NPF, BVOC emissions from the plants were not varied. Data with respect to the impact of NO_x on mass yields were only obtainable exploiting the natural variations of BVOC emissions from the plants ($[BVOC]_0$ varied between ∼ 44 and ∼ 73 µg m^{-3}). As a consequence, yields were based on the limited variations of $[BVOC]_0$.

Incremental mass yields were determined as described in Mentel et al. (2009). The maximum particle mass measured during the respective experiments was determined from the maximum volume assuming a density of 1.2 g cm^{-3}. Slopes of maximum particle mass concentrations as a function of consumed BVOC mass were taken as incremental mass yields. A yield of 11.7 ± 2 %, $R^2 = 0.81$, was determined for the data obtained without NO_x addition. An incremental mass yield of 12.6 ± 3 %, $R^2 = 0.65$, was determined for the experiments with NO_x addition when omitting the data obtained in the experiments with the two highest $[NO_x]_0$ for the regression analysis. Within the error limits, the same mass yields were determined with and without NO_x addition. For the experiments with the two highest $[NO_x]_0$ (103.5 and 69 ppb, BNR = 1.1 and 1.8, respectively) significant depletion of SOA mass formation was found (yields ∼ 1 %).

To analyze SOA mass formation as a function of BNR, the impacts of variable $[BVOC]_0$ had to be separated from impacts of $[NO_x]_0$. This was achieved by normalizing $[BVOC]_0$ to 65 µg m^{-3}. Normalization was conducted using the results from the linear regression analysis of data obtained without NO_x addition, which resulted in a mass yield of 0.117 (11.7 % see above). Considering that more than 95 % of the BVOCs introduced into the reaction chamber were oxidized

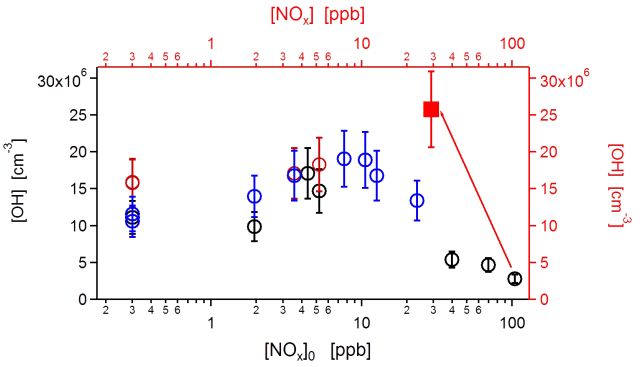

Fig. 6. OH concentrations measured during the first hour after switching on the TUV lamp in dependence of $[NO_x]_0$ (note logarithmic scale of x axis). The error in OH concentrations is estimated to be ±20 %. Brown circles represent OH measured at $[BVOC]_0 < 55\,\mu g\,m^{-3}$, blue circles those measured at $55 < [BVOC]_0 < 65\,\mu g\,m^{-3}$ and black circles those measured at $[BVOC]_0 > 65\,\mu g\,m^{-3}$. The red square shows the OH concentration measured for the highest NO_x addition ($[NO_x]_0 = 103.5$ ppb), 5 h after ignition of the TUV lamp. After that time new particle formation was observed, $[O_3]$ had increased to 85 ppb and $[NO_x]$ had decreased to 26 ppb.

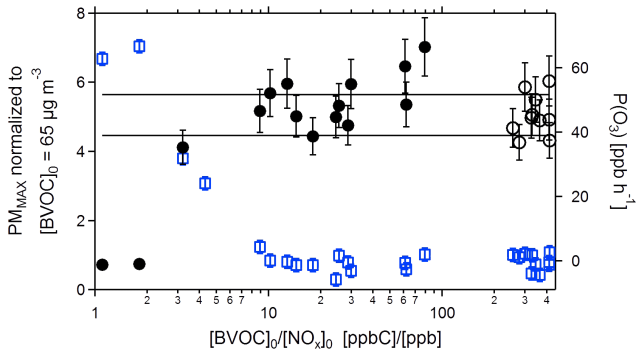

Fig. 7. PM_{max} normalized to $[BVOC]_0 = 65\,\mu g\,m^{-3}$ in dependence of BNR assuming incremental mass yield of 0.117. Solid circles show data from experiments with NO_x addition; open circles are from experiments without NO_x addition. The error in PM_{MAX},norm is mainly due to the extra- and interpolations to $[BVOC]_0 = 65\,\mu g\,m^{-3}$ and estimated to ±12 %. The black lines show the average $\pm 1\sigma$ standard deviation (upper/lower line) of the data without NO_x addition. For comparison $P(O_3)$ is shown (blue squares) as in Fig. 5. For one of the experiments (BNR = 4.3, $[NO_x]_0 = 23$ ppb) PM_{MAX} was not available. Therefore the number of data in Fig. 7 include one less than in Fig. 5.

$PM_{MAX,}$norm was calculated as

$$PM_{MAX,}\text{norm} = PM_{MAX,}\text{meas} + 0.117 \cdot (65 - [BVOC]_0). \quad (2)$$

In Eq. (2), PM_{max},meas is the maximum particle mass measured during individual experiments and PM_{max},norm is the particle mass that would have been obtained if $[BVOC]_0$ would have been $65\,\mu g\,m^{-3}$ during each of these experiments. $PM_{MAX,}$norm is shown in Fig. 7 as a function of BNR. The normalized data show still some scatter. However, as long as BNR > 10, PM_{max}norm was independent of NO_x within the error margins of the data. J_7 was affected at BNR < 30 (see Fig. 5 and compare ratio J_7 / PM_{max} in Table 1).

For a better overview, data obtained during the experiments using BVOC emissions from plants as SOA precursors are listed in Table 1. As shown in Table 1, the ratio J_7 / PM_{max} increased by about two orders of magnitude when BNR increased from 3 to 30 ppb C ppb^{-1}. At BNR > 30 J_7 / PM_{max} leveled out.

4.4 Experiments with α-pinene

UVA light and the ratio $[NO]/[NO_2]$ controlled by $J(NO_2)$ can influence NPF and SOA yields. Experiments were conducted to test whether the observed impacts of NO_x arise from NO or from NO_2 or from the UVA light ($\lambda > 350$ nm) in general. The experiments were conducted with α-pinene from a diffusion source in order to be independent of the day-to-day fluctuations of $[BVOC]_0$ observed for the real plant emissions. Details of the diffusion source are given in Mentel et al. (2009) and in Heiden et al. (2003). About 11 ppb of α-pinene were introduced into the reaction chamber. Particle formation was measured for α-pinene without NO_x addition and for $[NO_x]_0$ set to 3.3 or 7.0 ppb. Measurements were performed either without UVA light ($J(NO_2) = 0\,s^{-1}$) or with UVA light providing $J(NO_2) = 4.3 \times 10^{-3}\,s^{-1}$. In the first case all NO_x was converted to NO_2 while in the latter a significant fraction of NO was present in the reaction system.

Without NO_x addition ($[NO_x]_0 < 300$ ppt) we observed that the UVA light suppressed NPF as well as SOA mass formation. J_7 decreased from 373 to 139 $cm^{-3}\,s^{-1}$ and PM_{max} dropped from 6 to $2\,\mu g\,m^{-3}$. To remove the effect of the suppressions induced by UVA light, we normalized the data for the two different light conditions separately. As reference points we choose J_7 and PM_{max} as measured without NO_x addition with UVA light off ($J(NO_2) = 0\,s^{-1}$) and UVA light on ($J(NO_2) = 4.3 \times 10^{-3}\,s^{-1}$). Since the data were normalized separately for the two light conditions the impact of UVA light on NPF and SOA mass cancelled out. Figure 8 shows that the suppression of J_7 with NO_x addition was stronger at $J(NO_2) = 4.3 \times 10^{-3}\,s^{-1}$ than at $J(NO_2) = 0\,s^{-1}$. This suggests that NO is the NO_x component most responsible for suppression of new particle formation. The OH concentrations were not systematically affected by the addition of NO_x.

After eliminating NPF suppression by UVA light, the residual relative suppression of PM_{max} with increasing $[NO_x]$ was small (max. 50 %) and showed no systematic variation with $[NO_x]_0$. The suppression of PM_{max} was within the uncertainty of the data and small compared to the suppression of J_7. The lack of significant suppression of mass formation was consistent with the results obtained with the plant

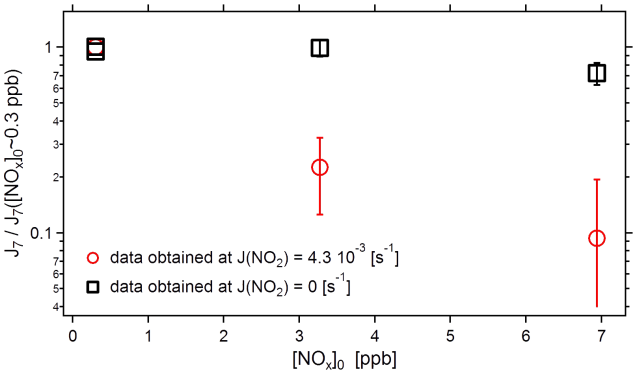

Fig. 8. J_7 normalized to J_7 measured at $[NO_x]_0 \sim 0$ ppb as a function of $[NO_x]_0$. Red circles: data points measured at $J(NO_2) = 4.3 \times 10^{-3}\,s^{-1}$, black squares: data measured at $J(NO_2) \sim 0\,s^{-1}$. In the presence of UVA light, suppression of J_7 by NO_x addition was more pronounced than in the absence of UVA light. As J_7 for $[NO_x] \sim 0.3$ ppb (reference points) was forced to be 1, no error limits are given for both reference points. Other errors are determined from error propagation setting the error for the reference points to zero. Note the logarithmic scale for J_7.

emitted BVOC mix. As all measurements with α-pinene were conducted at BNR > 15; suppression of SOA mass formation should thus not occur. It is therefore not possible to decide whether NO or NO_2 caused the suppression of PM_{max} in the BVOC mix at BNR < 10.

5 Discussion

5.1 Impact of NO_x on J_7

5.1.1 Comparison with literature data

We found a strong suppression of NPF with increasing NO_x for the BVOC mix emitted from Mediterranean species and dominated by monoterpenes. With BNR decreasing from 30 to 1.1 J_7 decreased by more than two orders of magnitude.

Limited data exist in the literature with respect to impacts of NO_x on NPF. Pandis et al. (1991) found nucleation thresholds for β-pinene in the range of 300 to 500 ppb C, which is quite high. According to Kroll et al. (2006) the high threshold found by Pandis et al. (1991) can be explained by high background NO concentrations. These high background NO concentrations might have suppressed RO_2 formation. Hence formation of PRP is also suppressed. From this Kroll et al. (2006) concluded that hydroperoxides formed in Reaction (R3a) are important for NPF. If so, NPF should be totally suppressed at high NO_x conditions as found in this study.

In contrast, Lim and Ziemann (2005) measured particle formation from OH initiated oxidation of long chain alkanes even at $[VOC]_0 / [NO_x]_0 < 0.05$. This would not be easily explained if PRP would be the only compounds involved in early particle formation. But Lim and Ziemann also observed that the particles formed in their experiments comprised mostly oxidation products of organic nitrates. The observation of Lim and Ziemann is in line with observations on the sesquiterpene–NO_x system by Ng et al. (2007b). Mechanisms of SOA formation from molecules with structures and chemical behavior different from that of monoterpenes may favor the $RONO_2$ route and may differ from those discussed here for monoterpenes.

5.1.2 Working hypothesis on the mechanism of NO_x impacts on NPF

Only when OH was produced from ozone photolysis we observed formation of new particles with diameters above 7 nm, otherwise NPF was insignificant. We conclude that OH is a necessary oxidant for NPF in the range of $[BVOC]_0$ applied here (see also Mentel et al., 2009; Kiendler-Scharr et al., 2009, 2012; Lang-Yona et al., 2010).

At high $[NO_x]_0$ conditions, NPF was not observed during the first hours of the experiments (as long as $[NO_x]$ was high), although OH concentrations reached about $2.6 \times 10^6\,cm^{-3}$ (see Table 1). Under atmospheric conditions, NPF is observed at comparable OH concentrations and even lower BVOC concentrations than those used here. We attribute the suppression of NPF to the presence of high $[NO_x]$ and not to a lack of [OH]. As a consequence, in the presence of NO_x, NPF must be suppressed by a mechanism other than the OH effect proposed for isoprene (Kiendler-Scharr et al., 2009).

This assumption is further supported by the observations of [OH] at the onset of NPF. At high $[NO_x]_0$ the chemical system developed on a timescale of hours and [OH] steadily increased in this time period (see Fig. 4). OH concentrations reached high levels of $2.2–2.6 \times 10^7\,cm^{-3}$ when NPF was observed (compare red square in Fig. 6). The threshold OH concentration was clearly higher than that measured at the onset of NPF at low to medium $[NO_x]_0$ (Table 1) but J_7 was orders of magnitude lower. The enhanced OH threshold for NPF in presence of NO_x implies that the mechanism responsible for the suppression of NPF by NO_x is superimposed to impacts of [OH].

Results of the experiment with α-pinene as SOA precursor were also consistent with this conclusion. In this experiment [OH] was not systematically affected by the addition of NO_x because the reactivity of the total mix increased by less than 20 %. But J_7 decreased by an order of magnitude confirming that there must have been another process suppressing J_7 by the addition of NO_x.

The experiment with α-pinene further confirmed that NO is mainly responsible for suppression of J_7. This is in accordance with the hypothesis that PRP are precursors in NPF: reactions of NO with peroxy radicals (Reaction R2) suppress the formation of PRP and therewith NPF. The same arguments apply for suppression of NPF as assumed for the suppression of SOA mass formation by NO_x (e.g., Pandis et

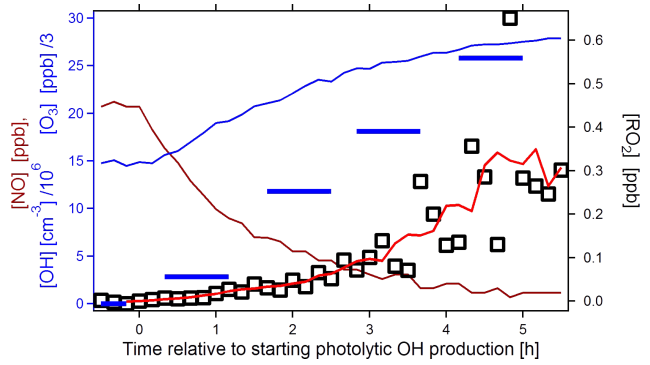

Fig. 9. Estimated $[RO_2]$ $(=\sum_i [RO_2{}^i])$ using deviation from PSS and an average rate constant $k_2 = 9 \times 10^{-12}\,cm^3\,s^{-1}$ for Reaction (R2). The open black squares show the original calculation, the red line shows the five point moving average of the $[RO_2]$ data (both right-hand *y* scales). The brown line shows the NO concentrations measured during the experiment, the blue bars indicate OH concentrations divided by 10^6 for clarity, and the blue line shows the ozone concentrations divided by 3 for clarity (left-hand *y* scale). New particle formation started 5 h after the TUV lamp was switched on. Then [NO] had decreased to ∼ 1 ppb and $[RO_2]$ had increased to ∼ 300 ppt. Errors in $[NO_x]$ (±8 %), $[O_3]$ (±2 ppb), and [OH] (±10 %), are estimated as before but not shown for clarity. Errors in absolute values of $[RO_2]$ are not shown because they are unknown. These errors depend on the error of the average rate constant for the mix, which is unknown.

al., 1991; Presto et al., 2005b; Kroll et al., 2006; Ng et al. 2007b).

5.1.3 Temporal development of the photochemical system

As suggested above, peroxy radicals play a crucial role for NPF. Their concentrations are difficult to measure, however, they can be estimated using the deviation of $\frac{[NO_2]}{[NO]}$ from the photo stationary steady state, PSS (for details see Supplement, Sect. 4). Figure 9 shows the estimated RO_2 concentrations for the experiment with the highest $[NO_x]_0$ (BNR = 1.1, first row in Table 1). At the early phase of the OH induced photochemistry, deviation of $\frac{[NO_2]}{[NO]}$ from PSS was insignificant but with progressing photochemistry $\frac{[NO_2]}{[NO]}$ deviated more and more from PSS.

Because k_2 is uncertain absolute numbers on $[RO_2]$ are also uncertain. Nevertheless, the systematic change in $\frac{[NO_2]}{[NO]}$ is obvious and implies that $[RO_2]$ increased with time during the high $[NO_x]_0$ experiments.

The increase of $[RO_2]$ is expected considering basic photochemistry: photochemical O_3 production increased $[O_3]$ and hence OH production rates ($J(O^1D)$ and $[H_2O]$ were constant). In parallel, $[NO_x]$ decreased due to higher loss rates by the NO_2+ OH reaction. With increasing production rates and decreasing loss rates, OH concentrations increased (Figs. 9, 4). Higher [OH] led to higher RO_2 production rates, $P(RO_2)$. In parallel, RO_2 losses in Reaction (R2) became less efficient with time because of decreasing [NO]. Similar as in the case of OH, increasing source strength and decreasing losses for RO_2 caused the increases in $[RO_2]$ over time for the experiments starting at high $[NO_x]_0$. In summary, the chemical system switched from high NO_x conditions to low NO_x conditions. NPF was not observed when [NO] was high. NPF was only observed when [NO] was low and $[RO_2]$ became high.

5.1.4 New particle formation in relation to photochemical ozone production

Photochemical ozone formation was insignificant for BNR > 10. However, $P(O_3)$ increased when BNR decreased from 10 to 1.1. In BVOC rich systems with BNR > 10 the main RO_2 losses proceeded via Reaction (R3), because RO_2 consumption by NO via Reactions (R2) could not compete. At low BNR $P(O_3)$ became significant, indicating that Reactions (R2) proceeded with considerable rates. This behavior is known from the classic empirical kinetic modeling approach's (EKMA) ozone isopleth diagram (e.g., Finlayson-Pitts and Pitts, 1986).

NPF exhibited an opposite behavior to $P(O_3)$; namely, J_7 decreased with decreasing BNR. J_7 dropped by more than two orders of magnitude when BNR decreased from 30 to 1.1. Obviously, increasing $[NO_x]_0$ had caused a switch of the chemical system from Reaction (R3) to Reaction (R2) (from the red to the blue arrows in Fig. 1).

Using BNR ($[BVOC]_0 / [NO_x]_0$) as a parameter is not the best choice but justified when comparing to literature using this terminology. However, in those experiments in which NPF was delayed substantially, the consumption of $[NO_x]$ by OH led to a different regime with lower $[NO_x]$ and higher $[BVOC] / [NO_x]$. Thus, NPF observed after long lag times is not related to $[NO_x]_0$, but to the actual $[NO_x]$. The approximately squared dependence of J_7 on BNR in Fig. 5 may be fortuitous at least for BNR < 10 with lag times exceeding several minutes. We therefore made use of Eq. (1), which relates $[RO_2]$ and $P(O_3)$.

From the overall increase of $P(O_3)$ for 10 > BNR > 1.1 in Fig. 5, we conclude that $P(O_3)$ is NO_x-limited in that BNR range. Moreover, $P(O_3)$ increases approximately linearly with decreasing BNR, indicating that the rate of Reaction (R2a) must also increase approximately linearly. $P(O_3)$ is thus a linear measure of Reaction (R2) and therefore also a measure of the $[RO_2]$ that is withdrawn from the PRP channels. According to our working hypothesis $P(O_3)$ is therefore also a measure of the RO_2 withdrawn from NPF and SOA mass formation. $P(O_3)$ as measured at the onset of NPF should therefore provide hints on the impacts of RO_2 on J_7.

Figure 10 shows a plot of $\ln(J_7)$ vs. $\ln(P(O_3))$. Linear regression analysis resulted in a slope of -1.6 ± 0.27

($R^2 = 0.87$). This slope indicates that J_7 and $P(O_3)$ are nonlinearly connected.

The observed relationship between J_7 and $P(O_3)$ indicated a mechanistic inverse coupling between J_7 and $P(O_3)$. Considering the competition of reaction pathways Reactions (R2) and (R3), the simplest way of explaining the coupling would be a direct involvement of PRP in NPF. Since $P(O_3)$ is a linear measure of $[RO_2]$ and P(PRP) is proportional to the square of $[RO_2]$, P(PRP) should decrease in a squared manner with respect to increases of $P(O_3)$. This would suggest power law dependence with a slope of -2, which is somewhat steeper than the measured slope. Nevertheless, losses of intermediate particle precursors apart from the pathway of new particle formation can easily explain attenuation of slopes for power law dependence. From the substantial nonlinearity indicated by the relationship between J_7 and $P(O_3)$ as well as from the substantial nonlinearity of the relationship between J_7 and BNR we conclude that PRP are involved in NPF.

However, there is an inconsistency in this analysis. Considering Eq. (1), it is obvious that an inverse squared dependence of P(PRP) on $P(O_3)$ can only be obtained if $[RO_2]$ is more or less constant. If so, constant $[RO_2]$ will certainly cause constant P(PRP). If P(PRP) would determine NPF in a simplistic fashion, J_7 should also be constant in the range $1.1 < BNR < 10$. However, J_7 changed by about two orders of magnitude. Hence P(PRP) and J_7 are not directly coupled.

To confirm the consequence of strictly applying Eq. (1) we calculated the peroxy radical concentrations at the onset of NPF for all experiments relative to the experiment with the highest NO_x addition (BNR = 1.1). Details of these calculations are given in the Supplement and we here summarize the basic result: at the onset of NPF, $[RO_2]$ was indeed quite constant in all experiments (see Supplement Table S1 and Sects. S4 and S5). Within the uncertainties of such calculations $[RO_2]$ did not vary by more than a factor of two and there were no systematic variations of $[RO_2]$ with variations of BNR.

Invariable $[RO_2]$ at high variability of J_7 suggested that J_7 was not determined by P(PRP). We therefore conclude that Reaction (R3) as depicted in Fig. 1 is not the rate limiting step for new particle formation (see also Supplement Sect. S6). PRP formed from first-generation peroxy radicals are not the vapors that directly aid NPF, probably because they do not reach supersaturations required to grow nanometer particles. This may be because their vapor pressures are too high or their production rates too small.

Evidence that the abundance of first-generation PRP does not limit the rates of new particle formation is supported by the suppression of J_7 in the range $10 < BNR < 30$ in absence of significant $P(O_3)$. Here NPF was still suppressed by an order of magnitude suggesting that reaction pathways leading to NPF were substantially affected by NO. The same amount of NO was not efficient enough to generate measurable $P(O_3)$ (see Fig. 5 and compare to Fig. 10). Inefficient $P(O_3)$ indicates that rates of Reaction (R2) are low and PRP production remain high. Suppression of J_7 by 90 % without significant increases in rates of Reaction (R2) can only be explained by compounds that are involved in NPF but do not significantly contribute to photochemical ozone formation.

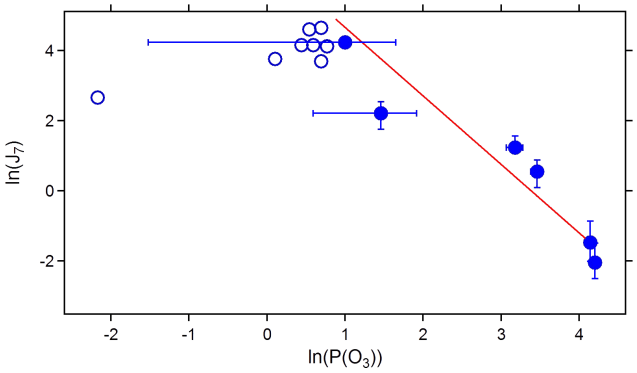

Fig. 10. Double logarithmic plot of J_7 ($cm^{-3}\,s^{-1}$) vs. $P(O_3)$ ($ppb\,h^{-1}$). Open circles are data obtained at $P(O_3) < 2.5\,ppb\,h^{-1}$, closed circles are data obtained at $P(O_3) > 2.5\,ppb\,h^{-1}$. Data pairs with $P(O_3) < 2.5\,ppb\,h^{-1}$ were regarded as error prone because $P(O_3)$ was calculated to $-0.15 \pm 2.5\,ppb\,h^{-1}$ when no NO_x was added although $P(O_3)$ was essentially zero. Therefore linear regression analysis was restricted to data points with $P(O_3) > 2.5\,ppb\,h^{-1}$. The slope of the linear regression line is -1.6 ± 0.27, $R^2 = 0.9$. Data points with formally negative $P(O_3)$ are not included in the plot. Error bars added only to data points used for the fit. Note that for $P(O_3)$ approaching the significance level, the error of the logarithm approaches infinity (∞).

The higher generation molecules produced by PRP oxidation may be a comprehensible explanation for the observed suppression of J_7 without photochemical ozone formation. These RO_2-like molecules must be abundant at much lower concentrations than first-generation RO_2 but capable of reacting with NO even faster than first-generation RO_2.

The assumption that higher generation RO_2-like molecules are produced from further oxidation is supported by another finding: as shown by Kiendler-Scharr et al. (2009), NPF dependence on [OH] exhibits power law dependence with an exponent of ~ 4. This power law dependence indicates that at least four OH radicals are consumed until new particles are formed from the oxidation of monoterpenes. The chemical system studied here is similar to that shown by Kiendler-Scharr et al. (2009). Hence, similar numbers of oxidation steps with OH are likely also needed here to produce the vapors that are able to grow nanometer particles. Formation of two first-generation peroxy radicals requires less than 4 OH radicals, at maximum one for each RO_2. The requirement of more oxidation steps by OH radicals is in accordance with the requirement of further PRP oxidation to produce the vapors directly involved in NPF.

Further oxidation of first-generation PRP may form the intermediate vapors that directly grow smaller particles to 7 nm

particles. However, these higher generation vapors are not yet identified. Maybe some of the high molecular weight oxidation products shown to be produced during α-pinene oxidation (Ehn et al., 2012; Zhao et al., 2013; Kulmala et al., 2013) are such vapors or precursors of them.

Despite of the unknown identity of these compounds, our data hint to some of their chemical properties and to the character of the rate limiting step of NPF:

- Essential gas phase precursors must be produced in a reaction chain induced by OH oxidation of BVOC: NPF was not observed without photolytic OH generation and from previous experiments we know that NPF increases with increasing $[BVOC]_0$ (Mentel et al., 2009). The vapors therefore must have been produced in an OH initiated reaction from the BVOC.

- The vapors capable of condensing on nanometer particles are produced by precursors with chemical properties similar to those of peroxy radicals: suppression of NPF by NO shows that the concentrations of the RO_2-like molecules are efficiently suppressed with increasing NO. Affinity to NO and chemical properties similar to those of peroxy radicals is the only explanation for the observed behavior.

- Rate limiting step in NPF from monoterpene oxidation is a permutation reaction: Reaction (R2) consumes one NO molecule and the inverse squared dependence of NPF on $P(O_3)$ shows that two molecules are involved in the rate limiting step. Either two of the RO_2-like molecules react among each other or one RO_2-like molecule reacts with a first-generation peroxy radical. However, it is a permutation reaction that limits the formation of a 7 nm particle and not a simple oxidation by OH or O_3.

5.2 Impact of NO_x on SOA mass formation

5.2.1 Comparison with literature data

We found SOA mass yields in the range of 12 %, which is substantially higher than the yields observed in Mentel et al. (2009) and in Lang-Yona et al. (2010) (4–6 %). The reason of this deviation is not clear. The previous determinations of SOA mass yields in our system were performed at a larger dynamic range of $[BVOC]_0$ together with a reliable determination of thresholds. In this study we tried to keep $[BVOC]_0$ as constant as possible to separate the effects of NO_x. $[BVOC]_0$ varied less than a factor of two and in particular the threshold was not reliably determinable. We therefore consider the $\sim$ 12 % yield not as an exact value but as an upper limit. However, impacts of NO_x on SOA mass formation were reliably determinable because the dynamic range of $[NO_x]_0$ spanned more than two orders of magnitude.

There are several studies on the impact of NO_x on particle mass formation (e.g., Pandis et al., 1991; Martín-Reviejo and Wirtz, 2005; Song et al., 2005; Presto et al., 2005b; Ng et al., 2007a, b; Kroll et al., 2006; Zhang et al., 2006). We restrict the comparison of our data with studies on BVOC. Table 2 gives examples for results obtained with respect to mass yields from BVOC oxidation in dependence of NO_x.

The BVOC mix emitted from the set of plants investigated here predominantly comprised of monoterpenes and we studied photooxidation without seed aerosol. Appropriate comparisons of our results are those to results of Pandis et al. (1991), Presto et al. (2005b), Ng et al. (2007b), Eddingsaas et al. (2012), and Kim et al. (2012) (lines below the table separator in Table 2).

Ng et al. (2007b), Eddingsaas et al. (2012), and Kim et al. (2012) qualitatively compared SOA mass yields from monoterpene photooxidation under low and high NO_x conditions (Ng et al.: BNR $\sim$ 1 and $\sim$ 400; Eddingsaas et al.: without NO_x addition and at NO_x $\sim$ 800 ppb; Kim et al.: BNR between $\sim$ 33 and $\sim$ 6). All these studies found that SOA yields were lower at low BNR than at high BNR. This is consistent with our results. Pandis et al. (1991) report increasing yields with BNR values from 1 to 15. For BNR > 15 they report decreasing yields with increasing BNR. Such a decrease at high BNR was not found here. But for BNR < 15, our results are in qualitative agreement with those of Pandis et al. (1991). Our data regarding impacts of NO_x on SOA mass formation are nearly identical to those of Presto et al. (2005b). For the BVOC mix investigated here, NO_x addition had no significant impact on SOA yield as long as BNR was above 10. Only for the two data points obtained at BNR < 3 was suppression of SOA yield obvious.

Decrease in SOA mass formation with decreasing BNR is attributed to the loss of peroxy radicals and the formation of organic nitrates (Reaction R2b). In case of monoterpene or isoprene oxidation, organic nitrates produced in Reaction (R2b) are expected to have higher volatility than products formed in the absence of NO_x (e.g., Presto et al., 2005b; Kroll et al., 2006). Thus, when more organic nitrates are formed, SOA formation should be lower than at low NO_x conditions.

In principle the routes via organic nitrates are possible. However, the degree of suppression in our experiments was substantially higher than can be explained by formation of organic nitrates. Of course organic nitrate formation is increasingly favored over PRP formation with increasing [NO]. But this holds only as long as $k_2 \cdot [NO] \cdot [RO_2] \approx k_3 \cdot [RO_2]^2$. If $k_2 \cdot [NO] \cdot [RO_2] >> k_3 \cdot [RO_2]^2$, organic nitrate formation is limited by RO_2. Adding more NO can then not produce more organic nitrates and cannot produce more ozone. For a given BVOC mixture the branching ratio of organic nitrate formation from reactions of alkylperoxy radicals with NO is fixed. Assuming that the data for α-pinene, β-pinene and limonene in the master chemical mechanism (MCM3.2) are applicable to our BVOC mix, we expect that about 25 % of the peroxy radicals can form organic nitrates via Reaction (R2b), the other 75 % form O_3 via Reaction (R2a). Scavenging of

Table 2. Impacts of NO_x on SOA formation from BVOC. PO, photooxidation; O_3, ozonolysis; S, seed aerosol used. BNR is the ratio $[BVOC]_0 / [NO_x]_0$ in ppb C ppb^{-1}.

Reference	SOA precursor	Observed effect on mass yield
Presto et al. (2005b)	α-pinene/O_3	Increase with increasing BNR up to BNR $\sim$ 10. No impact if BNR > 10.
Kroll et al. (2006)	Isoprene/PO/S	Increase with increasing BNR up to BNR $\sim$ 1. For BNR > 1 decrease with increasing BNR.
Ng et al. (2007b)	Longifolene/PO/S	Steady decrease with increasing BNR.
Eddingsaas et al. (2012)	α-pinene/PO/S	Increase with increasing NO_x.
H. Zhang et al. (2012)	Methacrolein/PO/S	Higher yield at higher BNR.
Pandis et al. (1991)	β-pinene /PO	Increase with increasing BNR up to $\sim$ 15. For BNR > 15 decrease with increasing BNR.
Presto et al. (2005b)	α-pinene /PO	Strong suppression when BNR falls below 4.5.
Ng et al. (2007b)	α-pinene/PO/S	Higher yield at higher BNR
	Aromadendrene /PO/S	Decrease with increasing BNR.
Eddingsaas et al. (2012)	α-pinene/PO	Higher yield at higher BNR.
Kim et al. (2012)	Limonene, α-pinene/PO	Higher yield at higher BNR.

about 25 % of the intermediates involved in SOA mass formation cannot lead to a drop of SOA mass formation by more than an order of magnitude even if organic nitrates would not at all contribute to particle mass formation. However, an order of magnitude reduction in PM_{max} was observed here for the highest NO_x conditions. The strong drop in PM_{max} must have other reasons.

Our measurements were made without seed aerosols and thus particle mass could not be accumulated without NPF before. Inhibition of NPF causes limitations in particle number density, particle surface, and particle volume precluding efficient condensation or solution of non-nucleating vapors (e.g., Kerminen et al., 2000). The observed suppression of PM_{max} at low BNR (see Fig. 7) may just be a consequence of foregoing suppression of NPF. Missing NPF could contribute to suppression of SOA mass production by NO_x in our setup, but would be in conflict to the results of experiments with seed aerosol (e.g., Kroll et al., 2006; Ng et al. 2007b). We therefore suppose that NO_x also affects SOA mass formation.

5.2.2 Impact of first-generation RO_2 on SOA yield

So far we cannot distinguish between NO or NO_2 as the NO_x component causing the reduction of SOA mass yields. In accordance to most of the other published data we assume that NO is responsible for suppression of PM_{max}. If so, changes in SOA mass formation by NO_x addition may be caused by impacts of NO on first-generation $[RO_2]$.

As shown above, $[RO_2]$ was not very sensitive to $[NO_x]_0$ suggesting that formation rates of first-generation PRP are not rate limiting for NPF. Similarly we can conclude that formation rates of first-generation PRP are also not rate limiting for SOA mass formation as SOA mass formed timely after NPF appeared, i.e., when $[NO_x] << [NO_x]_0$ in the high NO_x cases. Therefore, $[RO_2]$ and P(PRP) were similar in all cases when particle mass was formed. Again, presuming that particle mass formation is affected by NO_x, further PRP oxidation seems to be required to produce the condensing vapors aiding SOA mass formation. As in case of NPF, the highly oxidized compounds detected by Ehn et al. (2012) and Kulmala et al. (2013) are candidates of vapors aiding SOA mass formation.

As is obvious from the systematic change of J_7 / PM_{max} (Table 1), the chemical properties of vapors aiding mass formation is somewhat different from that of intermediates aiding NPF. If NO is the compound causing suppression of PM_{max}, suppression of J_7 at constant PM_{max} indicates that the vapors aiding NPF have higher affinity to NO than vapors aiding mass formation. A higher oxidative stage of the former might be the explanation for this.

6 Summary and conclusion

We found that increasing NO in an otherwise unchanged photochemical system favors photochemical ozone formation and suppresses new particle formation, suggesting a mechanistic connection between both processes. However, the behavior of NPF was too complex for a simplistic chemical mechanism that includes first-generation oxidation products only. Our data indicate that higher-generation intermediates are involved in NPF. These intermediates have similar chemical properties as peroxy radicals. They react with NO and they react among each other in permutation reactions forming low vapor pressure intermediates. This means that the formation rates of intermediates with vapor pressures low enough to allow condensation on nanoparticles are controlled by rates of permutation reactions. At least one of the reactants must be a higher-generation RO_2-like molecule.

From previous studies, we know that traces of H_2SO_4 in a range of 10^5–10^6 cm^{-3} are present in our system and H_2SO_4 might have acted as a nucleating agent also in the experiments described here. Nevertheless, volatile organic compounds were necessary for particles to reach diameters of 7 nm. As such, basic principles of RO_2 chemistry were suitable to explain the dynamic behavior of the chemical system including NPF.

Supplementary material related to this article is available online at http://www.atmos-chem-phys.net/14/2789/2014/acp-14-2789-2014-supplement.pdf.

Acknowledgements. The authors would like to acknowledge financial support by the integrated EU projects PEGASOS (Contract no. 265148) and ECLAIRE (Contract no. 282910).

The service charges for this open access publication have been covered by a Research Centre of the Helmholtz Association.

Edited by: B. Vogel

References

Atkinson, R.: Gas-phase tropospheric chemistry of volatile organic compounds: 1. Alkanes and alkenes, J. Phys. Chem. Ref. Data, 26, 215–290, 1997.

Betha, R., Spracklen, D. V., and Balasubramanian, R.: Observations of new aerosol particle formation in a tropical urban atmosphere, Atmos. Environ., 71, 340–351, 2013.

Dal Maso, M., Sogacheva, L., Aalto, P. P., Riipinen, I., Komppula, M., Tunved, P., Korhonen, L., Suur-Uski, V., Hirsikko, A., Kurten, T., Kerminen, V.-M., Lihavainen, H., Viisanen, Y., Hansson, H.-C., and Kulmala, M.: Aerosol size distribution measurements at four Nordic field stations: identification, analysis and trajectory analysis of new particle formation bursts, Tellus B, 59, 350–361, 2007.

Eddingsaas, N. C., Loza, C. L., Yee, L. D., Chan, M., Schilling, K. A., Chhabra, P. S., Seinfeld, J. H., and Wennberg, P. O.: α-pinene photooxidation under controlled chemical conditions – Part 2: SOA yield and composition in low- and high-NO_x environments, Atmos. Chem. Phys., 12, 7413–7427, doi:10.5194/acp-12-7413-2012, 2012.

Ehn, M., Junninen, H., Petäjä, T., Kurtén, T., Kerminen, V.-M., Schobesberger, S., Manninen, H. E., Ortega, I. K., Vehkamäki, H., Kulmala, M., and Worsnop, D. R.: Composition and temporal behavior of ambient ions in the boreal forest, Atmos. Chem. Phys., 10, 8513–8530, doi:10.5194/acp-10-8513-2010, 2010.

Ehn, M., Kleist, E., Junninen, H., Petäjä, T., Lönn, G., Schobesberger, S., Dal Maso, M., Trimborn, A., Kulmala, M., Worsnop, D. R., Wahner, A., Wildt, J., and Mentel, Th. F.: Gas phase formation of extremely oxidized pinene reaction products in chamber and ambient air, Atmos. Chem. Phys., 12, 5113–5127, doi:10.5194/acp-12-5113-2012, 2012.

Finlayson-Pitts, B. J. and Pitts, J. N.: Atmospheric chemistry: Fundamentals and experimental techniques, 611–618, Wiley-Interscience, New York, ISBN 0-471-88227-5, 1986.

Hallquist, M., Wenger, J. C., Baltensperger, U., Rudich, Y., Simpson, D., Claeys, M., Dommen, J., Donahue, N. M., George, C., Goldstein, A. H., Hamilton, J. F., Herrmann, H., Hoffmann, T., Iinuma, Y., Jang, M., Jenkin, M. E., Jimenez, J. L., Kiendler-Scharr, A., Maenhaut, W., McFiggans, G., Mentel, Th. F., Monod, A., Prévôt, A. S. H., Seinfeld, J. H., Surratt, J. D., Szmigielski, R., and Wildt, J.: The formation, properties and impact of secondary organic aerosol: current and emerging issues, Atmos. Chem. Phys., 9, 5155–5236, doi:10.5194/acp-9-5155-2009, 2009.

Heiden, A. C., Kobel, K., Langebartels, C., Schuh-Thomas, G., and Wildt, J.: Emissions of oxygenated volatile organic compounds from plants, part I: Emissions from lipoxygenase activity, J. Atmos. Chem., 45, 143–172, 2003.

Kerminen, V., Virkkula, A., Hillamo, R., Wexler, A., and Kulmala, M.: Secondary organics and atmospheric cloud condensation nuclei production, J. Geophys. Res., 105, 9255–9246, doi:10.1029/1999JD901203, 2000.

Kiendler-Scharr, A., Wildt, J., Dal Maso, M., Hohaus, T., Kleist, E., Mentel, Th. F., Tillmann, R., Uerlings, R., Schurr, U., and Wahner, A.: New Particle formation in forests inhibited by isoprene emissions, Nature, 461, 381–384, 2009.

Kiendler-Scharr, A., Andres, S., Bachner, M., Behnke, K., Broch, S., Hofzumahaus, A., Holland, F., Kleist, E., Mentel, Th. F., Rubach, F., Springer, M., Steitz, B., Tillmann, R., Wahner, A., Schnitzler, J.-P., and Wildt, J.: Isoprene in poplar emissions: effects on new particle formation and OH concentrations, Atmos. Chem. Phys., 12, 1021–1030, doi:10.5194/acp-12-1021-2012, 2012.

Kim, H., Barkey, B., and Paulson S. E.: Real refractive indices and formation yields of secondary organic aerosol generated from photooxidation of limonene and α-pinene: The effect of the HC/NO_x Ratio, J. Phys. Chem. A., 116, 6059–6067, 2012.

Kirkby, J., Curtius, J., Almeida, J., Dunne, E., Duplissy, J., Ehrhart, S., Franchin, A., Gagne, S., Ickes, L., Kurten, A., Kupc, A., Metzger, A., Riccobono, F., Rondo, L., Schobesberger, S., Tsagkogeorgas, G., Wimmer, D., Amorim, A., Bianchi, F., Breitenlechner, M., David, A., Dommen, J., Downard, A., Ehn, M., Flagan, R. C., Haider, S., Hansel, A., Hauser, D., Jud, W., Junninen, H., Kreissl, F., Kvashin, A., Laaksonen, A., Lehtipalo, K., Lima, J., Lovejoy, E. R., Makhmutov, V., Mathot, S., Mikkila, J., Minginette, P., Mogo, S., Nieminen, T., Onnela, A., Pereira, P., Petäjä, T., Schnitzhofer, R., Seinfeld, J. H., Sipila, M., Stozhkov, Y., Stratmann, F., Tome, A., Vanhanen, J., Viisanen, Y., Vrtala, A., Wagner, P. E., Walther, H., Weingartner, E., Wex, H., Winkler, P. M., Carslaw, K. S., Worsnop, D. R., Baltensperger, U., and Kulmala, M.: Role of sulphuric acid, ammonia and galactic cosmic rays in atmospheric aerosol nucleation, Nature, 476, 429–433, 2011.

Kroll, J. H., Ng, N. L., Murphy, S. M., Flagan, R. C., and Seinfeld, J. H.: Secondary organic aerosol formation from isoprene photooxidation, Environ. Sci. Technol., 40, 1869–1877, 2006.

Kulmala, M., Vehkamaki, H., Petajda, T., Dal Maso, M., Lauri, A., Kerminen, V. M., Birmili, W., and McMurry, P. H.: Formation and growth rates of ultrafine atmospheric particles: a review of observations, J. Aerosol. Sci., 35, 143–176, 2004a.

Kulmala, M., Kerminen, V. M., Anttila, T., Laaksonen, A., and O'Dowd, C. D.: Organic aerosol formation via sulphate cluster activation, J. Geophys. Res.-Atmos., 109, D04205, doi:10.1029/2003JD003961, 2004b.

Kulmala, M., Kontkanen, J., Junninen, H., Lehtipalo, K., Manninen, H. E., Nieminen, T., Petäjä, T., Sipilä, M., Schobesberger, S., Rantala, P., Franchin, A., Jokinen, T., Järvinen, E., Äijälä, M., Kangasluoma, J., Hakala, J., Aalto, P. P., Paasonen, P., Mikkilä, J., Vanhanen, J., Aalto, J., Hakola, H., Makkonen, U., Ruuskanen, T., Mauldin III, R. L., Duplissy, J., Vehkamäki, H., Bäck, J., Kortelainen, A., Riipinen, I., Kurtén, T., Johnston, M. V., Smith, J. M., Ehn, M., Mentel, Th. F., Lehtinen, K. E., Laaksonen, A., Kerminen, V.-M., and Worsnop, D. R.: Direct observation of atmospheric aerosol nucleation, Science, 339, 943–946, 2013.

Lang-Yona, N., Rudich, Y., Mentel, Th. F., Bohne, A., Buchholz, A., Kiendler-Scharr, A., Kleist, E., Spindler, C., Tillmann, R., and Wildt, J.: The chemical and microphysical properties of secondary organic aerosols from Holm Oak emissions, Atmos. Chem. Phys., 10, 7253–7265, doi:10.5194/acp-10-7253-2010, 2010.

Lim, Y. B., and Ziemann, P. J.: Products and mechanism of secondary organic aerosol formation from reactions of *n*-alkanes with OH radicals in the presence of NO_x, Environ. Sci. Technol., 39, 9229–9236, 2005.

Master Chemical Mechanism, MCM, version 3.2, http://mcm.leeds.ac.uk/MCM/roots.htt (last access: February 2014), 2013

Martín-Reviejo, M. and Wirtz, K.: Is benzene a precursor for secondary organic aerosol?, Environ. Sci. Technol., 39, 1045–1054, 2005.

Mentel, Th. F., Wildt, J., Kiendler-Scharr, A., Kleist, E., Tillmann, R., Dal Maso, M., Fisseha, R., Hohaus, Th., Spahn, H., Uerlings, R., Wegener, R., Griffiths, P. T., Dinar, E., Rudich, Y., and Wahner, A.: Photochemical production of aerosols from real plant emissions, Atmos. Chem. Phys., 9, 4387–4406, doi:10.5194/acp-9-4387-2009, 2009.

Mentel, Th. F., Kleist, E., Andres, S., Dal Maso, M., Hohaus, T., Kiendler-Scharr, A., Rudich, Y., Springer, M., Tillmann, R., Uerlings, R., Wahner, A., and Wildt, J.: Secondary aerosol formation from stress-induced biogenic emissions and possible climate feedbacks, Atmos. Chem. Phys., 13, 8755–8770, doi:10.5194/acp-13-8755-2013, 2013.

Metzger, A., Verheggen, B., Dommen, J., Duplissy, J., Prevot, A. S. H., Weingartner, E., Riipinen, I., Kulmala, M., Spracklen, D. V., Carslaw, K. S., and Baltensperger, U.: Evidence for the role of organics in aerosol particle formation under atmospheric conditions, P. Natl. Acad. Sci. USA, 107, 6646–6651, 2010.

Ng, N. L., Kroll, J. H., Chan, A. W. H., Chhabra, P. S., Flagan, R. C., and Seinfeld, J. H.: Secondary organic aerosol formation from *m*-xylene, toluene, and benzene, Atmos. Chem. Phys., 7, 3909–3922, doi:10.5194/acp-7-3909-2007, 2007a.

Ng, N. L., Chhabra, P. S., Chan, A. W. H., Surratt, J. D., Kroll, J. H., Kwan, A. J., McCabe, D. C., Wennberg, P. O., Sorooshian, A., Murphy, S. M., Dalleska, N. F., Flagan, R. C., and Seinfeld, J. H.: Effect of NO_x level on secondary organic aerosol (SOA) formation from the photooxidation of terpenes, Atmos. Chem. Phys., 7, 5159–5174, doi:10.5194/acp-7-5159-2007, 2007b.

Pandis, S., Paulson, S., Seinfeld, J., and Flagan, R.: Aerosol formation in the photooxidation of isoprene and β-pinene, Atmos. Environ., 25, 997–1008, 1991.

Presto, A. A., Huff Hartz, K. E., and Donahue, N. M.: Secondary organic aerosol production from terpene ozonolysis. 1. Effect of UV Radiation, Environ. Sci. Technol., 39, 7036–7045, 2005a.

Presto, A. A., Hartz, K. E. H., and Donahue, N. M.: Secondary organic aerosol production from terpene ozonolysis. 2. Effect of NO_x concentration, Environ. Sci. Technol., 39, 7046–7054, 2005b.

Riipinen, I., Pierce, J. R., Yli-Juuti, T., Nieminen, T., Häkkinen, S., Ehn, M., Junninen, H., Lehtipalo, K., Petäjä, T., Slowik, J., Chang, R., Shantz, N. C., Abbatt, J., Leaitch, W. R., Kerminen, V.-M., Worsnop, D. R., Pandis, S. N., Donahue, N. M., and Kulmala, M.: Organic condensation: a vital link connecting aerosol formation to cloud condensation nuclei (CCN) concentrations, Atmos. Chem. Phys., 11, 3865–3878, doi:10.5194/acp-11-3865-2011, 2011.

Riipinen, I., Yli-Juuti, T., Pierce, J. R., Petäjä, T., Worsnop, D. R., Kulmala, M., and Donahue, N. M.: The contribution of organics to atmospheric nanoparticle growth, Nat. Geosci., 5, 453–458, 2012.

Song, C., Na, K., and Cocker, D.: Impact of the hydrocarbon to NO_x ratio on secondary organic aerosol formation, Environ. Sci. Technol., 39, 3143–3149, 2005.

Zhang, H., Lin, Y-H., Zhang, Z., Zhang, X., Shaw, S. L., Knipping, E. L., Weber, R. J., Gold, A., Kamens, R., and Surratt, J. D.: Secondary organic aerosol formation from methacrolein photooxidation: roles of NO_x level, relative humidity and aerosol acidity, Environ. Chem., 9, 247–262, 2012.

Zhang, R., Khalizov, A., Wang, L., Hu, M., and Xu, W.: Nucleation and Growth of Nanoparticles in the Atmosphere, Chem. Rev., 112, 1957–2011, 2012.

Zhang, J. Y., Huff Hartz, K. E., Pandis S. N., and Donahue, N. M.: Secondary organic aerosol formation from limonene ozonolysis: Homogeneous and heterogeneous influences as a function of NO_x, J. Phys. Chem. A, 110, 11053–11063, 2006.

Zhao, J., Ortega, J., Chen, M., McMurry, P. H., and Smith, J. N.: Dependence of particle nucleation and growth on high-molecular-weight gas-phase products during ozonolysis of α-pinene, Atmos. Chem. Phys., 13, 7631–7644, doi:10.5194/acp-13-7631-2013, 2013.

Appendix A

Table A1. List of acronyms used in the text.

Acronym	Denotation
BNR	Ratio $[BVOC]_0 / [NO_x]_0$ [ppb C ppb^{-1}]
BVOC	Biogenic volatile organic compounds; here a mix of monoterpenes and isoprene
$J(NO_2)$	Photolysis frequency for NO_2; here constant $= 4.3 \times 10^{-3}$ [s^{-1}]
$J(O^1D)$	Photolysis frequency for O_3; here constant $= 9 \times 10^{-4}$ [s^{-1}]
NPF	New particle formation; here formation rate of 7 nm particles, J_7 [cm^{-3} s^{-1}]
PM_{MAX}	Maximum particle mass
$P(O_3)$	Ozone production rate [ppb h^{-1}], (1 ppb h^{-1} = 0.278 ppt s^{-1})
$P(RO_2)$	Production rate of peroxy radicals [ppb h^{-1}], (1 ppb h^{-1} = 0.278 ppt s^{-1})
PRP	Permutation reaction products as hydroperoxides, alkoxy radicals, alcohols, and carbonyl compounds
PSS	Photostationary steady state; relationship between NO and NO_2 in absence of volatile organic compounds and OH
P(PRP)	Production rate of permutation reaction products
SOA	Secondary organic aerosols
TUV lamp	Low pressure mercury lamp, 254 nm, termed according to the denomination of the manufacturer (Phillips)
$Y(O_3)$	Yield for ozone formation in RO_2+ NO reactions; here assumed to be ~ 0.75
$Y(RONO_2)$	Yield for organic nitrate formation in RO_2+ NO reactions; here assumed to be ~ 0.25